JOURNAL OF AIRCRAFT
Vol. 49, No. 1, January–February 2012

Multistage-Fusion Algorithm for Estimation of Aerodynamic Angles in Mini Aerial Vehicle

C. Ramprasadh* and Hemendra Arya†
Indian Institute of Technology Bombay, Powai, Mumbai, Maharashtra, 400 076, India

DOI: 10.2514/1.C031322

This research work is inspired by the fact that a mini aerial vehicle with low-aspect-ratio wings (aspect ratio less than 2) has nonlinear lift curves and does not stall sharply, as compared with high-aspect-ratio wings. This paper presents a data fusion algorithm for estimating the aerodynamic angles in a mini aerial vehicle that has low-aspect-ratio wings. The true states of the aircraft motion are generated using a flight simulation program, and a zero-mean white noise is added to a few of these states for sensor simulation. Using the simulated sensors, in the first stage, Euler angles are estimated using an extended Kalman filter algorithm. The estimated Euler angles are further used with accelerometer, angular rates, magnetometer measurements, and the airspeed V for estimation of aerodynamic angles at higher angles of attack. This paper also proposes a novel pseudoestimation technique and also discusses three different schemes of estimation of angle of attack and sideslip angle. Effect of drift in gyro measurements in the angle-of-attack and sideslip-angle estimation is studied. When sensor bias/drift is present, it was observed that there is a bias of more than 10 deg present in the estimated aerodynamic angles. A new modification is proposed in which the pseudoestimation of angle of attack and sideslip angle is used as measurement in the second-stage extended Kalman filter. This reduces the estimation bias and the mean error in both angle of attack and sideslip angle, and it is below 1 deg.

Nomenclature

C	=	measurement matrix
C_D	=	coefficient of drag
C_L	=	coefficient of lift
C_l	=	moment coefficient in the x direction
C_m	=	moment coefficient in the y direction
C_n	=	moment coefficient in the z direction
C_x	=	force coefficient in the x direction
C_Y	=	coefficient of side force
C_y	=	force coefficient in the y direction
C_z	=	force coefficient in the z direction
F	=	system state matrix
F_x	=	total force along the body x axis
F_y	=	total force along the body y axis
F_z	=	total force along the body z axis
I_{xx}, I_{yy}, I_{zz}	=	moment of inertia
I_{xy}, I_{yz}, I_{xz}	=	product of inertia
J, f, f_1, f_2, g_1, g_2	=	generic functions
J_a	=	Jacobian
J_{ad}	=	advance ratio
K_k	=	Kalman gain at kth instant
L	=	total moment along the body x axis
M	=	total moment along the body y axis
m	=	mass of the mini aerial vehicle
N	=	total moment along the body z axis
n	=	engine rpm
P_k	=	estimation error covariance matrix at kth instant
p	=	roll rate
Q_k	=	process-noise covariance matrix at kth instant
q	=	pitch rate
R_k	=	measurement noise covariance matrix at kth instant
r	=	yaw rate
T	=	thrust
u	=	velocity along the body x axis
$\mathbf{u}$	=	input vector
u_{Euler}	=	control vector for attitude estimation
V	=	airspeed
v	=	velocity along the body y axis
W	=	weight of the mini air vehicle
w	=	velocity along the body z axis
w_g	=	stochastic noise vector
x	=	state vector
x_{Euler}	=	state vector for attitude estimation
x_e, y_e, z_e	=	coordinates representing the position of the aircraft
x_k	=	state vector at kth instant
y	=	measurement vector
y_{Euler}	=	measurement vector for attitude estimation
α	=	angle of attack
α_{NR}	=	angle of attack from Newton–Raphson solution
α_{pseudo}	=	angle-of-attack pseudoestimate
β	=	sideslip angle
β_{NR}	=	sideslip angle from Newton–Raphson solution
β_{pseudo}	=	sideslip-angle pseudoestimate
δ_a	=	aileron input
δ_e	=	elevator input
δ_r	=	rudder input
θ	=	pitch angle
Φ_k	=	discrete state transition matrix at kth instant
φ	=	roll angle
ψ	=	yaw angle
$\wedge$	=	estimated quantity
$-$	=	prior value
$\cdot$	=	time derivative

Presented at the 49th AIAA Aerospace Sciences Meeting, Orlando, FL, 4–7 January 2011; received 23 November 2010; revision received 2 August 2011; accepted for publication 15 August 2011.

*Research Scholar, Aerospace Engineering Department; crprasadh@aero.iitb.ac.in.

†Associate Professor, Aerospace Engineering Department; arya@aero.iitb.ac.in.

I. Introduction

THIS paper focuses on the development of a sensor fusion and estimation algorithm for the purpose of estimating the

aerodynamic angles in a mini aerial vehicle (MAV). The aerodynamic angles are very critical for operation in a high-angle-of-attack region. These aerodynamic angles are not directly measured by adding separate sensor units in MAVs due to weight constraint. Further, the sensors used in MAVs are of low cost and accuracy, and they provide noisy information. The application of low-accuracy sensors makes state estimation challenging, and the sensor suite also does not include units that measure angle of attack (AOA) and sideslip angle (SSA) [1,2]. Estimation of AOA and SSA is the first step toward designing any control law using the aerodynamic angles as feedback parameters. Thus, it is crucial to have a good estimate when it comes to their use in the feedback loop [3]. Oosterom and Babuska [4] propose a virtual AOA sensor and use the nonlinear Takagi–Sugeno fuzzy model. Here, the authors describe about two models for estimating AOA, including the above-mentioned fuzzy model. The other model is a white box linear time-varying model. Both of these models combined give the estimate of AOA. Perry et al. [5] have presented algorithm for estimation of AOA under high dynamics on small unmanned aerial vehicles (UAVs). They have presented the results of high-angle-of-attack flight exhibiting linearity in lateral dynamics and nonlinearity in longitudinal and directional dynamics [5,6]. Their paper also describes the challenges in modeling of flight dynamics at high angles of attack. Literature shows that the estimation of AOA and SSA could be done to an accuracy level of within 1.6 and 0.8 deg, respectively, at a confidence level of 95% [5]. Johnson and Lind [6] have developed an error model for AOA and SSA that gives us an idea of the variances of the error. A number of studies are also are found in the literature related to the estimation of aerodynamic angles applied to a range of various aircraft such as F16 [7], UAVs [5], and small commercial aircraft [4].

In the current work, estimation of AOA and SSA in a MAV using a multistage estimation algorithm using the simulated measurements of rate gyros, accelerometers, pressure sensors, and magnetometer is presented. It may be noted that these are the typical measurements that are available in autonomous MAVs. We have generated these measurements with a flight simulation program and adding zero-mean white Gaussian noise with appropriate true states of the aircraft. Sensor drift has also been considered in the gyro measurements. This paper proposes three different schemes of estimation algorithms and compares the results. Scheme 1 is a novel Newton–Raphson solver technique, scheme 2 is an extended Kalman filter (EKF) algorithm that includes the complete aerodynamic data, and scheme 3 is another EKF without considering the aerodynamic data. The results are compared with respect to the error statistics of the estimated AOA and SSA.

II. Problem Formulation

We have considered the general six-degree-of-freedom equations of motion of a rigid-body aircraft for modeling and simulation of the MAV. The force and moment equations are derived from basic Newtonian mechanics:

$$\mathbf{F} = m\left(\frac{\partial \mathbf{V}}{\partial t} + \Omega \times \mathbf{V}\right) \tag{1}$$

$$\mathbf{M} = \frac{\partial(\mathbf{I}\cdot\Omega)}{\partial t} + \Omega \times (\mathbf{I}\cdot\Omega) \tag{2}$$

where

$$\mathbf{V} = [\,u \quad v \quad w\,]^T \qquad \Omega = [\,p \quad q \quad r\,]^T$$
$$\mathbf{F} = [\,F_x \quad F_y \quad F_z\,]^T \qquad \mathbf{M} = [\,L \quad M \quad N\,]^T$$

where $\mathbf{F}$ is the total force vector, $\mathbf{M}$ is the total moment vector, and $\mathbf{I}$ is the inertia tensor of the rigid body. These equations form the main part of the simulation model. m' is the mass of the MAV, which is constant in our case. These equations are represented as a nonlinear state-space system:

$$\dot{x} = f(x, \mathbf{F}(t), \mathbf{M}(t)) \tag{3}$$

Table 1 MAV data ($m = 0.3$ kg)

Moment of inertia		Other geometric data	
I_{xx}	1.506×10^{-3} kgm^2	Overall length	0.3 m
I_{yy}	1.640×10^{-3} kgm^2	Overall height	0.155 m
I_{zz}	0.227×10^{-3} kgm^2	Wing span	0.3 m
I_{xy}	0	Area	0.0618 m^2
I_{yz}	0	MAC	0.211 m
I_{xz}	0.0363×10^{-3} kgm^2	Aspect ratio	1.45

where

$$\mathbf{F} = g_1(x(t), \mathbf{u}(t), w_g(t)) \tag{4}$$

$$\mathbf{M} = g_2(x(t), \mathbf{u}(t), w_g(t)) \tag{5}$$

Here, x is the state vector, $\mathbf{u}$ is the input vector, and w_g is process noise, and t is the time. The state vector is defined as follows:

$$x = [\,V \quad \alpha \quad \beta \quad p \quad q \quad r \quad \psi \quad \theta \quad \varphi \quad x_e \quad y_e \quad H\,]^T \tag{6}$$

where $H = -z_e$.

The input vector is

$$\mathbf{u} = [\,\delta_e \quad \delta_a \quad \delta_r \quad n\,]^T \tag{7}$$

The system dynamics equations for the above-mentioned state vector are taken from [8]. The aerodynamic forces and moments depend upon number of variables. The aerodynamic characteristics of the MAV are represented using the dimensionless aerodynamic coefficients that are associated with the stability and control derivatives. This results in the complicated nonlinear relation between each variable in the aerodynamic forces and moments. Using these fundamental concepts, a MATLAB® code has been developed for the flight simulation of the MAV, and the true states are generated. Several of these true states (such as V, p, q, r, B_x, B_y, B_z, A_x, A_y, and A_z) are superimposed with a zero-mean white Gaussian noise, with specific standard deviations. This is done in order to simulate noisy sensor measurement, which may be used for the estimation of the aerodynamic angles.

The multistage-fusion algorithm has been implemented for a typical MAV whose longitudinal aerodynamic coefficients are obtained from wind-tunnel data. The geometric and inertia details of the MAV are given in Table 1.

The MAV data in our simulation used 0.3 kg mass and a wing span of 0.3 m, valid for an elevator range of ± 18 deg. The wing area is 0.0618 m^2. The aerodynamic coefficients and engine thrust are expressed as follows:

$$T = \frac{4}{\pi^2}\rho n^2 D^4[-0.0948J_{\text{ad}}^2 + 0.058J_{\text{ad}} + 0.0761] \tag{8}$$

where

$$J_{\text{ad}} = \frac{V}{nD} \qquad D = 0.1 \text{ m}$$

$$C_L = 0.1748 + 2.453\alpha - 1.691\alpha^2 + 29.986\alpha^3 - 49.245\alpha^4 - 0.3638\delta_e^2 + 0.7405\delta_e \tag{9}$$

$$C_Y = -0.7678\beta + \frac{0.3}{2V}(-0.124p + 0.3666r) - 0.02956\delta_a + 0.1158\delta_r \tag{10}$$

$$C_D = 0.08712 - 0.05593\alpha + 3.4825\alpha^2 + 0.2258\delta_e^2 + 0.1471\delta_e \tag{11}$$

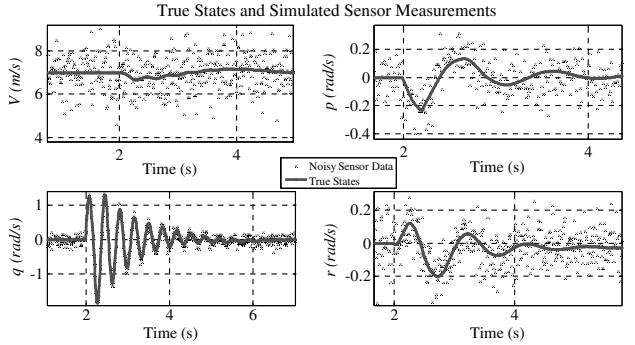

Fig. 1 True states and the simulated noisy states taken as measurements for the estimation of aerodynamic angles.

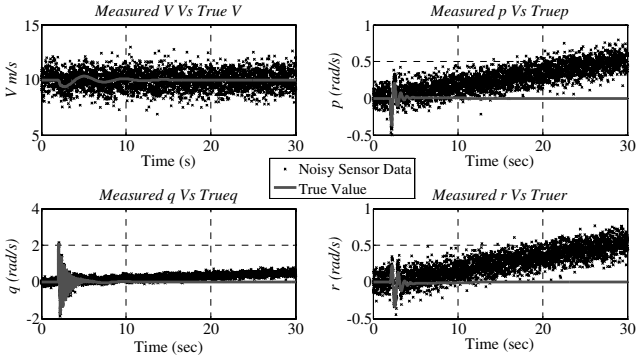

Fig. 2 True states and the simulated noisy states with gyro drift taken as measurements for the estimation of aerodynamic angles.

$$C_l = -0.0618\beta + \frac{0.3}{2V}(-0.5045p + 0.1695r) - 0.09917\delta_a + 0.006934\delta_r \tag{12}$$

$$C_m = 0.0385 - 0.59977\alpha - 1.27402\alpha^2 + 0.1587\delta_e^2 + 1.5894\delta_e \tag{13}$$

$$C_n = 0.006719\beta + \frac{0.3}{2V}(-0.1585p - 0.1112r) - 0.003872\delta_a - 0.08265\delta_r \tag{14}$$

Note that there is a limitation on the minimum airspeed (which is 6.25 m/s, with a corresponding maximum AOA of 22.89 deg) below which flight simulation was not carried out. The main reason for unsuccessful flight simulation is that the trim algorithm is unable to converge at a solution due to the fact that the elevator deflection range exceeds the maximum limit in the high AOA region. This results in the flight not being in steady trim condition. Figure 1 shows the simulated sensor data without gyro drift, whereas Fig. 2 shows the simulated sensor data with gyro drift of 1 deg/s. Table 2 provides the details about the standard deviation of sensor noise that are assumed for simulating the sensors.

Table 2 Sensor error standard deviations ($g = 9.81$ m/s^2)

Measurement	Sensor	Full-scale value	SD = 1% of full scale
V	Pressure sensor	4000 Pa	0.8081 m/s
p	Rate gyro	600 deg/s	0.1047 rad/s
q	Rate gyro	600 deg/s	0.1047 rad/s
r	Rate gyro	600 deg/s	0.1047 rad/s
A_x	Accelerometer	4 g	0.04 g
A_y	Accelerometer	4 g	0.04 g
A_z	Accelerometer	4 g	0.04 g

III. Multistage Estimation Scheme

The proposed multistage estimation involves stage 1, attitude estimation, and stage 2, aerodynamic-angle estimation.

Figure 3 shows the block diagram of the proposed estimations schemes. Stage one constitutes two methods of attitude estimation, which are 1) AM1, in which the attitude angles are estimated from the accelerometer and rate gyro outputs, and 2) AM2, in which the attitude angles are estimated from the accelerometer, rate gyro and magnetometer outputs. Similarly, stage 2 of the estimation has been implemented using three types of schemes: 1) ES1, which is a Newton–Raphson solver that estimates the aerodynamic angles considering the corresponding state equations as simultaneous nonlinear algebraic equations and weighted angular rates are later added; 2) ES2, which is an EKF algorithm that uses the complete aerodynamic data; and 3) ES3, which is another EKF that does not use the aerodynamic data and instead considers only the body-axis velocities as states. The attitude estimation method without magnetometer measurements (AM1) has been cascaded with ES1 and ES2, and the attitude estimation method involving magnetometer is used in ES3, as shown in Fig. 3. When the sensor drift is present in order to improve the estimates of AOA and SSA obtained from ES3, we propose to couple ES1 as pseudomeasurements with ES3, whose results are also presented and discussed in detail.

A. Extended Kalman Filter Design for Attitude Estimation

The outputs of the accelerometer along the body axes at the center of gravity, usually called the specific forces, are considered in the first method of estimation of attitude angles. The accelerometer output equations are as given below:

$$A_x = (F_x - F_{x\text{grav}})/W \tag{15}$$

$$A_y = (F_y - F_{y\text{grav}})/W \tag{16}$$

$$A_z = (F_z - F_{z\text{grav}})/W \tag{17}$$

These specific forces are taken from the flight simulation and a zero-mean white noise is added, as depicted in Table 2. An EKF estimation algorithm has been implemented. The state vector and measurement vector are written as follows. The attitude dynamic equations as given in [8] have been used for these two methods of estimation.

Method 1 (AM1) is attitude estimation without magnetometer measurement [9]. The state vector is

$$x_{\text{Euler}} = [\theta \quad \varphi]^T$$

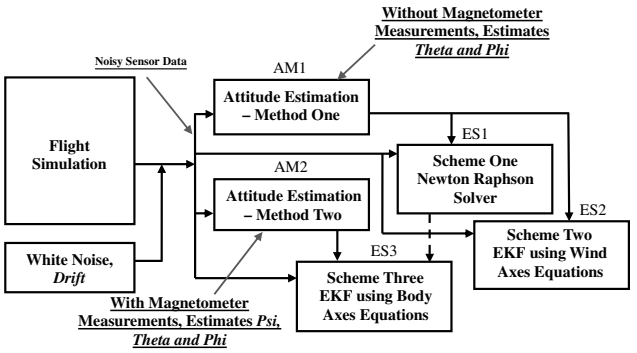

AM1 = Attitude Estimation Method 1 and AM2 = Attitude Estimation Method 2.
ES1 = Estimation Scheme 1, ES2 = Estimation Scheme 2 and ES3 = Estimation Scheme 3

Fig. 3 Block diagram of different schemes for attitude and aerodynamic-angle estimation.

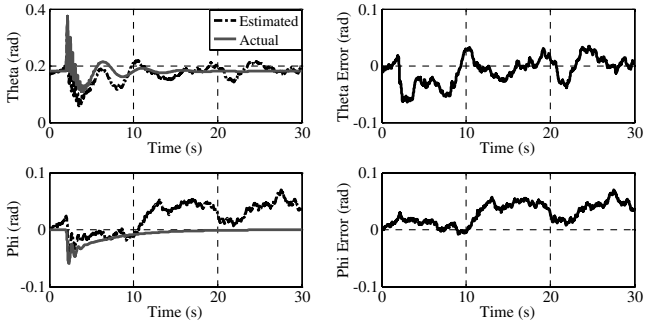

Fig. 4 Actual-vs-estimate attitude angles for airspeed of 10 m/s using the first method without magnetometer measurements.

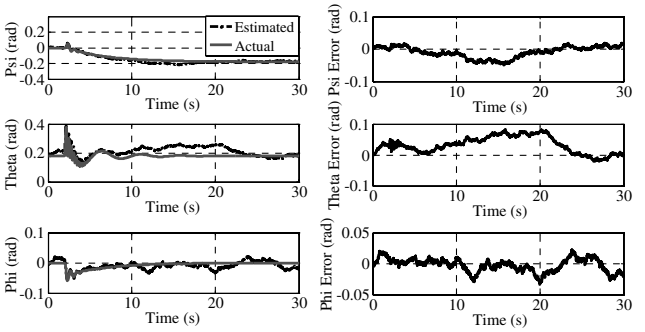

Fig. 5 Actual-vs-estimate attitude angles for airspeed of 10 m/s using the second method including magnetometer measurements.

the control vector is

$$u_{\text{Euler}} = [\,p \quad q \quad r\,]^T$$

and the measurement vector is

$$y_{\text{Euler}} = [\,A_x \quad A_y \quad A_z\,]^T$$

Method 2 (AM2) is attitude estimation with magnetometer measurements [10]. The state vector is

$$x_{\text{Euler}} = [\,\psi \quad \theta \quad \varphi\,]^T$$

the control vector is

$$u_{\text{Euler}} = [\,p \quad q \quad r\,]^T$$

and the measurement vector is

$$y_{\text{Euler}} = [\,A_x \quad A_y \quad A_z \quad B_x \quad B_y \quad B_z\,]^T$$

The estimation of attitude angles is shown here for an impulse input of amplitude 0.05 rad applied for 0.2 s on the elevator and aileron at an airspeed of 10 m/s. Figure 4 shows the estimated pitch and roll angles using AM1, and Fig. 5 shows the estimated pitch, roll, and yaw angles using AM2. Table 3 presents the statistical information on the estimated attitude angles.

Table 3 Error statistics of attitude estimation in degrees[a]

	Method 1		Method 2		
Quantity	Pitch	Roll	Yaw	Pitch	Roll
Mean error	−0.45	1.64	−0.55	1.89	−0.13
SD of error	1.32	1.06	0.99	1.57	0.62
Peak error	1.98	4.02	1.03	4.72	1.26

[a]For airspeed 10 m/s and for δ_e of 0.05 rad and δ_a of 0.05 rad for 0.2 s impulse.

B. Estimation of Aerodynamic Angles

Three types of estimation schemes are adopted for the estimation of AOA and SSA in the second stage. These estimation schemes are explained in detail in the coming sections. All three schemes were tested with and without the gyro drift. The results show that because of the sensor drift, the scheme ES3 exhibits a very high estimation bias and the estimates are not reliable. To reduce this estimation bias we propose to bring in the estimates of ES1 as pseudomeasurements of AOA and SSA in ES3. The results show satisfactory improvements in the estimated AOA and SSA.

1. *Scheme 1 (ES1): Newton–Raphson Solver*

In the ES1 methodology, the state vector is

$$x = [\,\alpha \quad \beta\,]^T$$

the measurement vector is

$$y = [\,V \quad p \quad q \quad r \quad \theta \quad \varphi\,]^T$$

and the method of estimation is the novel Newton–Raphson solver algorithm [11].

A Newton–Raphson solver is employed to solve two simultaneous nonlinear algebraic equations while equating $\dot{\alpha}$ and $\dot{\beta}$ equations to q and $-r\cos\alpha$, respectively. The $\dot{\alpha}$ and $\dot{\beta}$ equations for the system are given below:

$$\dot{\alpha} = \frac{1}{V\cos\beta}\left(-\frac{F_x}{m}\sin\alpha + \frac{F_z}{m}\cos\alpha\right) + q - (p\cos\alpha + r\sin\alpha)\tan\beta \tag{18}$$

$$\dot{\beta} = \frac{1}{V}\left(-\frac{F_x}{m}\cos\alpha\sin\beta + \frac{F_y}{m}\cos\beta - \frac{F_z}{m}\sin\alpha\sin\beta\right) + p\sin\alpha - r\cos\alpha \tag{19}$$

Writing $\dot{\alpha} \approx q$ and $\dot{\beta} \approx -r\cos\alpha$ in Eqs. (18) and (19), respectively, reduces to

$$\frac{1}{V\cos\beta}\left(-\frac{F_x}{m}\sin\alpha + \frac{F_z}{m}\cos\alpha\right) - (p\cos\alpha + r\sin\alpha)\tan\beta = 0 \tag{20}$$

$$\frac{1}{V}\left(-\frac{F_x}{m}\cos\alpha\sin\beta + \frac{F_y}{m}\cos\beta - \frac{F_z}{m}\sin\alpha\sin\beta\right) + p\sin\alpha = 0 \tag{21}$$

These algebraic equations are solved for α and β using the Newton–Raphson method. Here,

$$F_x = f(\alpha, \delta_e, \theta, \varphi, n)$$

$$F_y = f(\beta, p, r, \delta_a, \delta_r, \theta, \varphi)$$

$$F_z = f(\alpha, \delta_e, \theta, \varphi)$$

Rewriting the above equations as

$$f_1(x) = \frac{1}{V\cos\beta}\left(-\frac{F_x}{m}\sin\alpha + \frac{F_z}{m}\cos\alpha\right) - (p\cos\alpha + r\sin\alpha)\tan\beta \tag{22}$$

$$f_2(x) = \frac{1}{V}\left(-\frac{F_x}{m}\cos\alpha\sin\beta + \frac{F_y}{m}\cos\beta - \frac{F_z}{m}\sin\alpha\sin\beta\right) + p\sin\alpha \tag{23}$$

This is a nonlinear system of equations, which can be defined in the vector form as

$$f(x) = \begin{bmatrix} f_1(x) \\ f_2(x) \end{bmatrix} \tag{24}$$

where

$$x = \begin{bmatrix} \hat{\alpha}_{\mathrm{NR}} \\ \hat{\beta}_{\mathrm{NR}} \end{bmatrix} \tag{25}$$

Finding a solution for the above nonlinear system of equations $f(x)$ involves finding a solution such that every equation in the nonlinear system is 0. Approximating f using the first-order Taylor expansion in a neighborhood of a point $x_k \in \Re^2$. The Jacobian matrix $J(x_k) \in \Re^{2x2}$ to $f(x)$ evaluated at x_k is given by

$$J_a = \begin{bmatrix} \frac{\partial f_1}{\partial \alpha} & \frac{\partial f_1}{\partial \beta} \\ \frac{\partial f_2}{\partial \alpha} & \frac{\partial f_2}{\partial \beta} \end{bmatrix} \tag{26}$$

$$f(x_k) = f(x_k) + J(x_k) + \mathcal{O}(\|p\|^2) \tag{27}$$

By setting the right-hand side of the above equation to zero and truncating the series with first-order terms alone, we obtain

$$J(x_k) = -f(x_k) \tag{28}$$

The Newton–Raphson algorithm, as explained above, has been implemented. Setting $k = 0$, we initialize the algorithm with an initial guess of α and β equal to the trim values. Then the iteration starts by computing $J(x_k)$ and $f(x_k)$ and solving $J(x_k) = -f(x_k)$ until a converged solution occurs. The above algorithm provides us the estimated values of α_{NR} *and* β_{NR} at every instant. The Newton–Raphson solution of AOA and SSA are shown in Figs. 6 and 7, respectively. The estimation results are shown here for an impulse input of amplitude 0.05 rad applied for 0.2 s on the elevator and aileron at an airspeed of 10 m/s.

The Newton–Raphson solution captures major part of the translational dynamics. To capture the rotational kinematics that were earlier removed from Eqs. (18) and (19), weighted angular rates are added with the Newton–Raphson solution and written as follows:

$$\alpha_{\mathrm{pseudo}} = \alpha_{\mathrm{NR}} + (\mathrm{TC}_1 * \Delta t * q) \tag{29}$$

$$\beta_{\mathrm{pseudo}} = \beta_{\mathrm{NR}} - (\mathrm{TC}_2 * \Delta t * r * \cos(\alpha_{\mathrm{pseudo}})) \tag{30}$$

Here, TC_1 and TC_2 are tuning constants, and Δt is the time step. The values of TC_1 and TC_2 are to be obtained by numerical experimentation. These constants are found to be 1.75 and 0.001 in this case. The Newton–Raphson algorithm converges within two iterations for a tolerance of 10^{-2}. Figures 8 and 9 show the estimates of AOA and SSA after implementing Eqs. (29) and (30).

2. *Scheme 2 (ES2): EKF Estimation Algorithm Using Aerodynamic Data*

In the ES2 methodology, the state vector is

$$x = [V \quad \alpha \quad \beta \quad p \quad q \quad r]^T$$

the measurement vector is

$$y = [V \quad p \quad q \quad r]^T$$

and the method of estimation is the extended Kalman filter.

The system equations in the wind axis were considered, as mentioned earlier, from [8]. The six-state model is used and the system matrices are found. Then a six-state discrete-time EKF algorithm for the estimation of aerodynamic angles has been realized as follows.

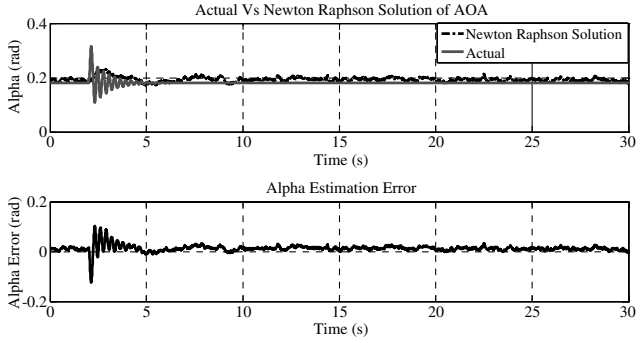

Fig. 6 Actual vs Newton–Raphson solution of AOA for airspeed of 10 m/s.

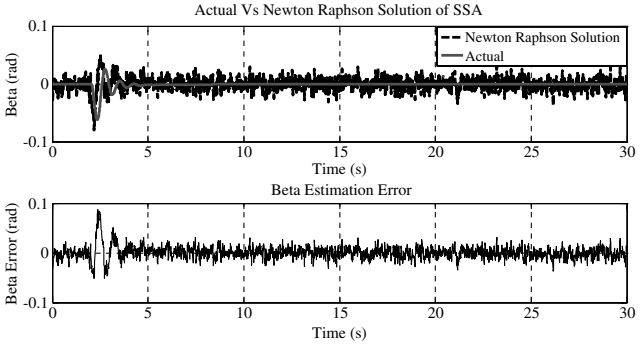

Fig. 7 Actual vs Newton–Raphson solution of SSA for airspeed of 10 m/s.

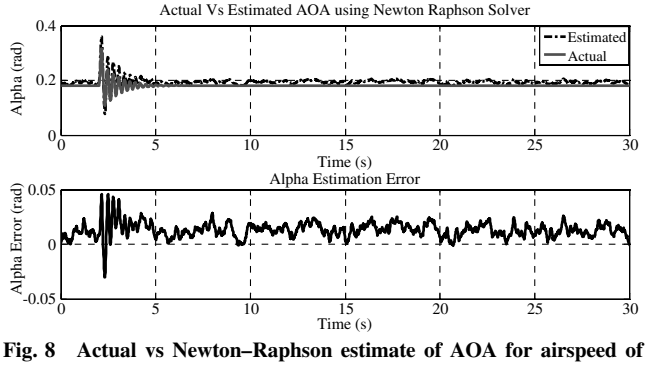

Fig. 8 Actual vs Newton–Raphson estimate of AOA for airspeed of 10 m/s.

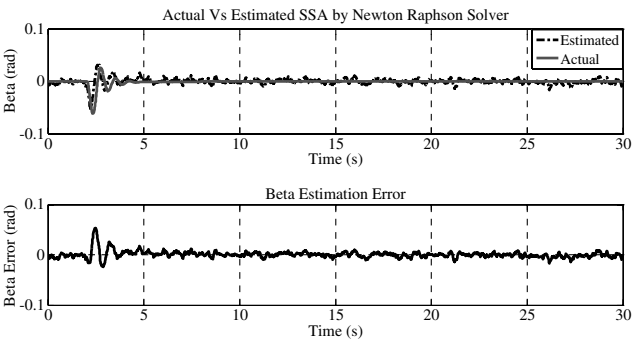

Fig. 9 Actual vs Newton–Raphson estimate of SSA for airspeed of 10 m/s.

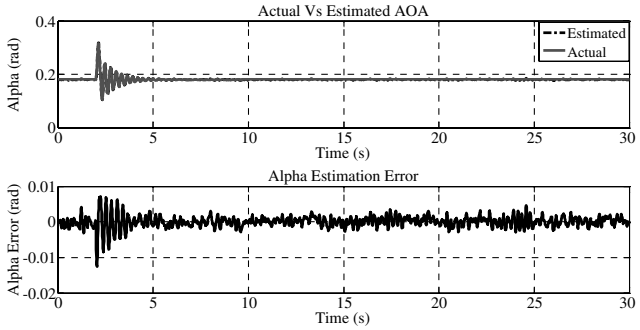

Fig. 10 Actual vs estimate of AOA without sensor drift for airspeed of 10 m/s and its error dynamics.

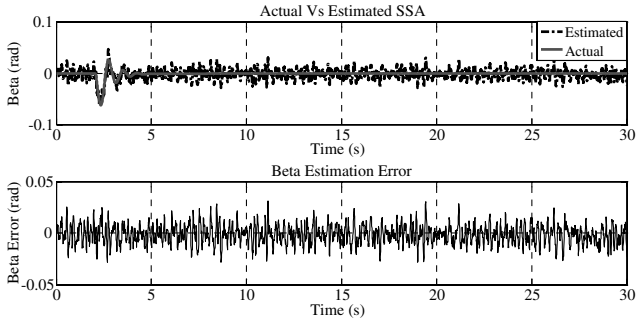

Fig. 11 Actual vs estimate of SSA without sensor drift for airspeed of 10 m/s and its error dynamics.

Initialize the state vector and state covariance matrix:

$$\hat{x}_0^- \quad \text{and} \quad P_0^-$$

1) Compute the Kalman gain matrix from state covariance and estimated measurement covariance:

$$K_k = P_k^- C_k^T [C_k P_k^- C_k^T + R_k]^{-1} \tag{31}$$

2) Multiply the prediction error vector by Kalman gain matrix to get state correction vector and update the state vector:

$$x_k^- = \hat{x}_k^- + K_k[y_k - c_k(\hat{x}_k^-)] \tag{32}$$

3) Update the error covariance:

$$P_k = [I - K_k C_k] P_k^- \tag{33}$$

4) Predict the new state vector and state covariance matrix:

$$\hat{x}_k^- = f_{k-1}(\hat{x}_{k-1}^-) \tag{34}$$

$$P_{k+1}^- = \Phi_k P_k \Phi_k^T + Q_k \tag{35}$$

5) Obtain the linear approximation equations for system and measurement matrices through the relations

$$F = \left.\frac{\partial f_k}{\partial x}\right|_{x=\hat{x}_k^-} \qquad C_k = \left.\frac{\partial c_k}{\partial x}\right|_{x=\hat{x}_k^-} \tag{36}$$

$$\Phi_k = I + FT_s \tag{37}$$

The state estimates are propagated forward by integrating the state equations using first-order Euler integration method. The estimated aerodynamic angles using the above-explained EKF are plotted in Figs. 10 and 11. The estimates exhibit high accuracy. ES2 is an EKF algorithm that includes the aerodynamic data and captures the system well. Figures 12 and 13 show the results with a gyro drift of 1 deg /s. The results are convincing with respect to the mean and standard deviation of the estimation error, which are less than 1 deg, and a peak error of around 5 deg using ES2.

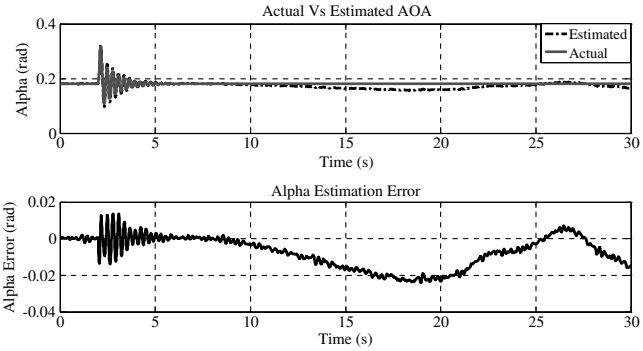

Fig. 12 Actual vs estimate of AOA with sensor drift for airspeed of 10 m/s and its error dynamics.

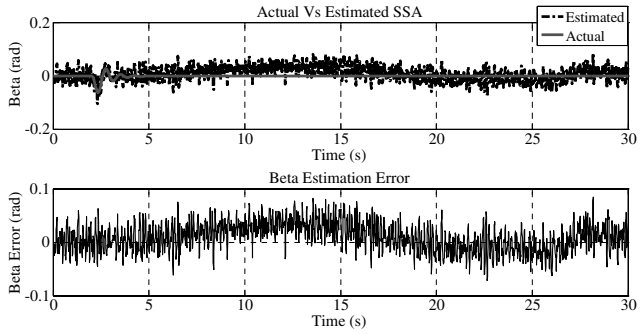

Fig. 13 Actual vs estimate of SSA with sensor drift for airspeed of 10 m/s and its error dynamics.

3. Scheme 3 (ES3): EKF Estimation Algorithm Without Using Aerodynamic Data

In the ES3 methodology, the state vector is

$$x = [\,u \quad v \quad w\,]^T$$

the measurement vector is

$$y = [\,V \quad \dot{x}_e \quad \dot{y}_e \quad \dot{z}_e\,]^T$$

and the method of estimation is the extended Kalman filter.

ES3 is a simple scheme as the number of states are only 3. Note that the ground velocity measurements are assumed to be available at every system equation update that is 10 ms. As explained earlier, we have used the system dynamics equations in the body axes, as given in [8]. The states u, v, and w are first estimated and then the aerodynamic angles are estimated, as given in Eqs. (38) and (39):

$$\alpha = \tan^{-1}\left(\frac{w}{u}\right) \tag{38}$$

$$\beta = \tan^{-1}\left(\frac{v}{\sqrt{u^2 + w^2}}\right) \tag{39}$$

Figures 14 and 15 show the estimated AOA and SSA using ES3 without gyro drift. But note that this particular scheme is highly vulnerable to sensor noise. It was observed that higher the sensor noise, the lower the quality of estimation. ES3 does not allow 1% standard deviation in the sensor noise, as depicted in Table 2. Instead, a 0.1% standard deviation was considered. It is also observed that even with a lower level of sensor noise, if gyro drift is present, the estimation errors are very high. Thus, we propose to couple ES1

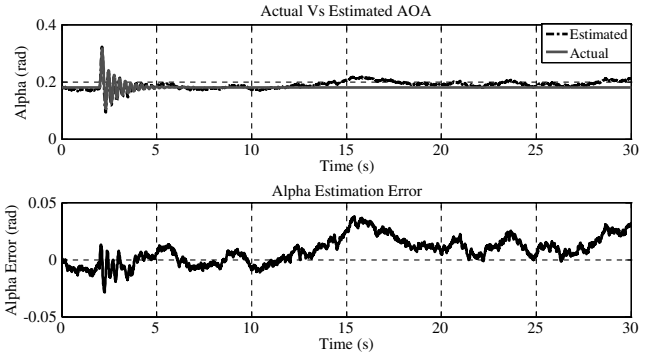

Fig. 14 Actual vs estimate of AOA without sensor drift for airspeed of 10 m/s and its error dynamics using scheme 3 with 0.1% standard deviation (SD) sensor noise.

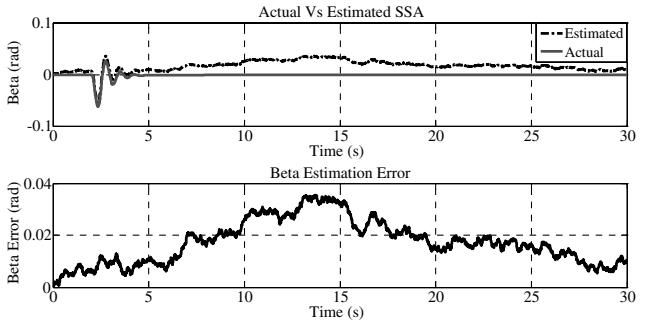

Fig. 15 Actual vs estimate of SSA without sensor drift for airspeed of 10 m/s and its error dynamics using scheme 3 with 0.1% SD sensor noise.

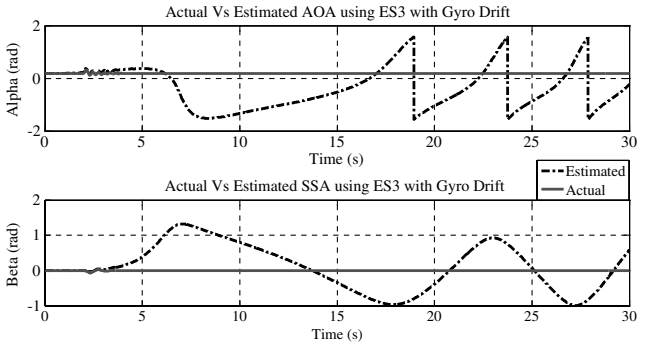

Fig. 16 Actual vs estimate of AOA and SSA with sensor drift for airspeed of 10 m/s using scheme 3.

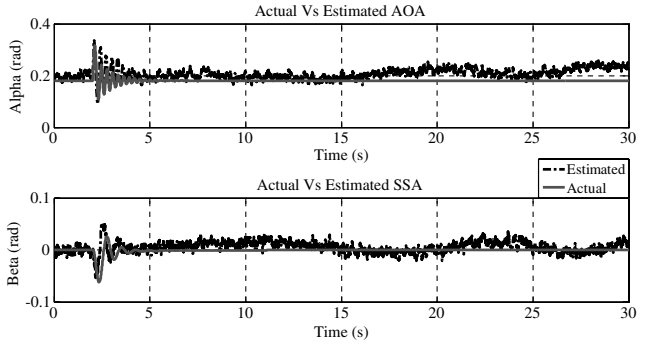

Fig. 17 Actual vs estimate of AOA and SSA with sensor drift for airspeed of 10 m/s using scheme 3 implemented with pseudomeasurement.

estimates of AOA and SSA as pseudomeasurements with ES3. The coupling of ES1 estimates as pseudomeasurements of AOA and SSA in ES3 makes the measurement vector as

$$[V \quad \alpha_{\text{pseudo}} \quad \beta_{\text{pseudo}} \quad \dot{x}_e \quad \dot{y}_e \quad \dot{z}_e]^T$$

Figure 16 shows the estimated AOA and SSA using ES3 with sensor drift, which has an unacceptable error. Figure 17 shows the results of estimated AOA and SSA after coupling ES1 and ES3. This result is quite convincing with respect to the quality of estimation. The results show the estimates of AOA and SSA considering a 1% standard deviation in sensor noise with a gyro drift of 1 deg/s, as it was considered in ES1 and ES2. It establishes that the use of pseudomeasurements of AOA and SSA in ES3 not only reduces the estimation error due to the sensor drift, but also provides the liberty of

Table 4 Error statistics of estimated AOA and SSA in degrees without sensor drift

Quantity	Scheme 1	Scheme 2	Scheme 3	Scheme 3 with pseudomeasurement
For a given δ_e of 0.05 rad for 0.2 s impulse				
Mean error in AOA	0.68	−0.01	0.73	0.86
SD in AOA error	0.91	−0.09	0.96	0.88
Peak error in AOA	1.96	0.38	6.13	6.02
Mean error in SSA	−0.002	0.003	1.83	0.13
SD in SSA error	0.27	0.55	1.05	0.33
Peak error in SSA	0.91	2.09	5.36	1.35
For a given δ_e and δ_a of 0.05 rad for 0.2 s impulse				
Mean error in AOA	0.75	0.0006	−0.49	0.75
SD in AOA error	0.40	0.11	0.64	0.55
Peak error in AOA	2.43	0.80	1.58	5.15
Mean error in SSA	0.07	0.03	0.57	0.08
SD in SSA error	0.44	1.14	0.90	0.43
Peak error in SSA	4.04	4.50	2.39	−1.66

Table 5 Error statistics of estimated AOA and SSA in degrees with sensor drift

Quantity	Scheme 1	Scheme 2	Scheme 3	Scheme 3 with pseudomeasurement
For a given δ_e of 0.05 rad for 0.2 s impulse				
Mean error in AOA	4.48	0.23	−31.01	1.48
SD in AOA error	2.35	0.16	69.63	1.09
Peak error in AOA	9.96	0.67	79.63	6.07
Mean error in SSA	2.88	0.20	−2.06	0.32
SD in SSA error	1.67	0.60	29.95	0.52
Peak error in SSA	6.10	2.21	89.91	2.10
For a given δ_e and δ_a of 0.05 rad for 0.2 s impulse				
Mean error in AOA	2.87	−0.41	−22.26	1.48
SD in AOA error	1.27	0.49	49.29	1.10
Peak error in AOA	5.45	0.78	79.63	6.95
Mean error in SSA	2.96	0.51	4.11	0.35
SD in SSA error	1.67	1.48	36.44	0.68
Peak error in SSA	6.10	4.84	74.28	5.04

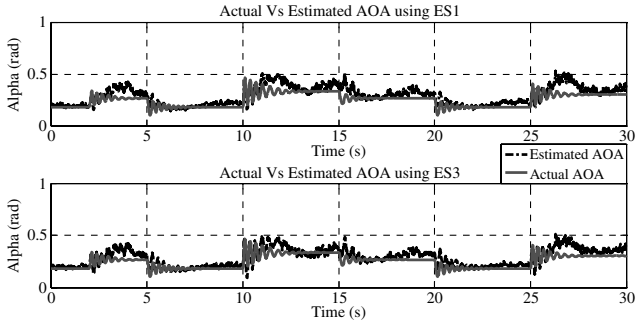

Fig. 18 Comparison of actual vs estimate of AOA for various trim airspeeds with gyro drift using ES1 and ES3 with pseudomeasurement.

using noisy sensors. The peak error remains around 6 deg, which is reduced from a very high value of more than 65 deg.

IV. Results and Discussion

The results presented in Tables 4 and 5 show the estimation error statistics with and without gyro drift, respectively, for an airspeed of 10 m/s. An independent elevator impulse as well as for a combined elevator and aileron impulse of 0.05 rad amplitude for 0.2 s were given and the error statistics were extracted. It is observed from the error statistics that scheme ES2 is the most accurate one as compared with schemes ES1 and ES3. In addition, to check the efficacy of the schemes, various control inputs were given. For example, Fig. 18 shows the estimated AOA and SSA from ES1 alone and ES3 coupled with the ES1 pseudomeasurements for inputs switching between various trim airspeeds. It is established that scheme ES1 provides a reasonably good estimates, even at higher-angle-of-attack region and the error statistics are of similar nature, as explained earlier. On the other hand, it is also note d that scheme ES3 is highly sensitive to sensor error and drift. But the proposed coupling of ES1 and ES3 brings out a comprehensive improvement in the estimated aerodynamic angles by ES3. It is also worth indicating that ES3 also provides the body-axis velocity estimates, along with the aerodynamic angles. ES1 helps to improve the estimates of u, v, and w in ES3, even when sensor drift is present.

The performance of all the schemes was also evaluated for sinusoidal variation in the control surface inputs. The error statistics are satisfactory, but there is a lead in the estimated aerodynamic angles as compared with their true values. This may be due to the kinematic addition of the pitch rate and the yaw rate, as given in Eqs. (29) and (30). One more concern is that the peak error also stands at a higher value of more than 5 deg. It has been attempted to reduce the peak error by two approaches. The first approach is to tune TC1 and TC2, and the second approach is to increase the convergence tolerance of the Newton–Raphson solution to 10^{-3}. The former approach helps to reduce the peak error but introduces bias in the estimate, whereas the latter helps only in bringing down the mean error. The schemes were also tested for performance at various airspeeds ranging from 6.25 to 22 m/s, and the errors are within the ranges as specified in this paper.

V. Conclusions

A novel estimation technique, based on Newton–Raphson solver, is proposed for the estimation of aerodynamic angles. The algorithm has been evolved considering the basic nonlinear dynamical model of AOA and SSA for their estimation. The results obtained are satisfactory. A sensor drift in the gyro gets propagated further when the body-axis dynamic equations are considered, as explained in scheme 3, resulting in unacceptable error and standard deviation in the estimated AOA and SSA. The present paper establishes that providing the Newton–Raphson-based estimates to scheme 3 as pseudomeasurements improves the quality of estimation of AOA and SSA. The presented work does not consider the effects of wind turbulence, which is an important factor in the estimation of aerodynamic angles. The turbulence effects may be taken up in the future to check the efficacy of the proposed estimation schemes.

Acknowledgment

We greatly acknowledge the National Aerospace Laboratories, Bangalore, for providing us the mini aerial vehicle aerodynamic data generated through wind-tunnel tests.

References

[1] de La Parra, S., and Angel, J., "Low Cost Navigation System for UAV's," *Aerospace Science and Technology*, Vol. 9, No. 6, 2005, pp. 504–516. doi:10.1016/j.ast.2005.06.005

[2] Jung, D.-W., and Tsiotras, P., "Modeling and Harware-in-the-Loop Simulation for a Small Unmanned Aerial Vehicle," AIAA Conference and Exhibit, Rohnert Park, CA, AIAA Paper 2007-2768, 2007.

[3] Lee, S.-H., and Park, Y.-M., "System Identification of DragonFly UAV via Bayesian Estimation," http://cs229.stanford.edu/proj2006/LeePark-SystemIdentificationofDragonFlyUAVviaBayesianEstimation.pdf

[4] Oosterom, M., and Babuska, R., "Virtual Sensor for the Angle-of-Attack Signal in Small Commercial Aircraft," *IEEE International Conference on Fuzzy Systems*, IEEE, Piscataway, NJ, 2006, pp. 1396–1403.

[5] Perry, J., Mohamed, A. H., Johnson, B., and Lind, R., "Estimating Angle of Attack and Sideslip Angle Under High Dynamics on Small UAVs," *ION GNSS Conference*, Savannah, GA, Sept. 16–19 2008.

[6] Johnson, B., and Lind, R., "High Angle-of-Attack Flight Dynamics of Small UAVs," 47th AIAA Aerospace Sciences Meeting, AIAA Paper 2009-0061, Orlando, FL, Jan. 5–8 2009.

[7] Zeis, J. E., Jr., "Angle of Attack and Sideslip Estimation Using an Inertial Reference Platform," M.S. Thesis, School of Engineering, Air Force Institute of Technology, Wright-Patterson AFB, OH, June 1988.

[8] Stevens, B. L., and Lewis, F. L., *Aircraft Control and Simulation*, Wiley, New York, 1992, chaps. 1, 2.

[9] Eldredge, A. M., "Improved State Estimation for Miniature air Vehicles," M.S. Thesis, Brigham Young University, Provo, UT, 2006.

[10] Zhu, R., Sun, D., Zhou, Z.-Y., and Wang, D.-Q., "A Linear Fusion Algorithm for Attitude Determination Using Low Cost MEMS-Based Sensors," *Measurement*, Vol. 40, No. 3, April 2007, pp. 322–328. doi:10.1016/j.measurement.2006.05.020

[11] Ramprasadh, C., and Arya, H., "Multi-Stage Fusion Algorithm for Estimation of Aerodynamic Angles in a Mini Aerial Vehicle," 49th AIAA Aerospace Sciences Meeting, AIAA Paper 2011-1287, Orlando, FL, Jan. 4–7 2011.